Nanoscale

Effects of Catalyst Droplets on Wire Growth and Resulting Branched Structures during VLS Growth

Journal:	*Nanoscale*
Manuscript ID	NR-COM-12-2019-010695.R1
Article Type:	Communication
Date Submitted by the Author:	27-Feb-2020
Complete List of Authors:	Song, Miao; Pacific Northwest National Laboratory, Physical and Computational Sciences Directorate Zhang, Youtian; Rice University, Materials Science and NanoEngineering Chun, Jaehun; Pacific Northwest National Laboratory, Experimental & Computational Engineering Hu, Shenyang; Pacific Northwest National Laboratory, Energy and Environment Directorate Tang, Ming; Rice University, Materials Science and NanoEngineering Li, Dongsheng; Pacific Northwest National Laboratory, Physical and Computational Sciences Directorate

Nanoscale

COMMUNICATION

Effects of Catalyst Droplets on Wire Growth and Resulting Branched Structures during VLS Growth

Received 00th January 20xx,
Accepted 00th January 20xx

DOI: 10.1039/x0xx00000x

www.rsc.org/

Miao Song,[a] Youtian Zhang[b], Jaehun Chun[a], Shenyang Hu[c], Ming Tang[b], Dongsheng Li*[a]

Vapor-liquid-solid (VLS) method is vastly employed to grow hierarchical structures with unique properties. However, key questions remain, such as what controls the branched structures and what the roles of catalyst droplet size are during the growth. Here, an in-depth understanding of the kinetics of the nucleation, growth, and subsequent coalescence processes of Bi liquid catalyst droplets is provided by direct observation of PbSe branched wire growth in an environmental transmission electron microscope. This brings a kinetic control of the branch density by varying the parameters, such as temperature. In addition, the dependence of wire growth rate on the catalyst droplet size is revealed, i.e., the smaller the catalyst size the larger the wire growth rate, unlike the wire growth controlled by Gibbs-Thomson effect, possibly due to different mass transport pathways and atomic surface diffusion. These results extend the fundamental understanding of the VLS growth mechanism of branched structures and benefit the structure design of hierarchical materials with tailored properties.

Complex hierarchical structures have unique properties and wide applications[1-4]. For example, hyperbranched PbSe nanowire networks presented the branching density related charge carrier transport properties[5], and the unique branched α-Fe_2O_3/SnO_2 nano-heterostructures are responsible for superior electrochemical performance[6]. Understanding the growth mechanisms of hierarchical structures enables the control of crystal structures[7, 8] and thus their properties.

Vapor-liquid-solid (VLS) method was extensively employed to grow hierarchical structures[5, 9, 10] However, questions remain regarding mechanisms of branched nanostructure growth, such as controlling factors of branch density, which is closely tied to the catalyst droplet formation process. Although *in situ* transmission electron microscopy (TEM) technique has been widely used in VSL growth study, key information on the nucleation and formation process of catalyst droplets is still missing because the limited space of the *in situ* experiments[5, 8, 11] cannot supply sufficient growth precursors and catalyst for branches to grow[5, 9].

In addition, there has been a controversy about the relationship between the wire growth rate and catalyst droplet size. For example, Givargizov[12] and Kikkawa [13] independently concluded that the Si nanowires with the smaller diameters grew more slowly (positive correlation) due to the Gibbs-Thomson effect. On the contrary, Nebol'sin, et al.,[14] found a negative correlation for Si wires grown at various temperatures. Kodambaka, et al.,[15] proposed that the growth rate is independent of catalyst droplet size, based on observation of one single Si nanowire growth at different times. This controversy would be probably caused by difficulties in maintaining the complex experimental conditions for comparison. Dayeh and Picraux[16] reported that the thicker the wire or the bigger the catalyst droplet size the faster the growth rate due to the Gibbs-Thomson effect, based on the simultaneous growth of Ge nanowires with different sizes of liquid Au catalyst droplets at same location. However, the size effect on the growth rate of compound wires g is still not well understood, such as GaAs (negative correlation)[17], InAs (negative correlation)[18,19], GaP (positive correlation)[20], due to the complex reactions involving multiple precursors and their partial pressures and mass transport pathways, etc[18, 20]. Here, we designed a VLS growth via multi-steps in *in situ* TEM experiments to overcome the aforementioned limitation. We employed PbSe as a model system to investigate the nucleation and growth process of liquid catalyst droplets on sidewalls of PbSe wires and the subsequent size-related growth kinetics of branches.

[a] Physical and Computational Sciences Directorate, Pacific Northwest National Laboratory, Richland, WA 99352, USA. E-mail: Dongsheng.Li2@pnnl.gov

[b] Department of Materials Science and NanoEngineering, Rice University, Houston, TX 77024, USA.

[c] Energy and Environment Directorate, Pacific Northwest National Laboratory, Richland, WA 99352, USA

†Electronic Supplementary Information (ESI) available: [Experimental, nucleation and growth of catalyst droplets on PbSe crystal, the calculated theoretical ratio of the catalyst droplet diameter and the PbSe wire width, evolution of PbSe wire width, structure and composition analysis of branched structures, evolution of partial pressure, estimation of the equilibrium contact angle, calculation of de-wetting process of catalyst liquid thin film, facet surface at high temperatures]. See DOI: 10.1039/x0xx00000x

PbSe branched wires were grown by providing sufficient Bi catalyst via multi-steps under N_2 gas environment (Fig. 1a-c). During step 1, PbSe wires first grew on a TEM grid (Fig. 1d-f) in a sandwiched cell. We defined these wires as the 1st PbSe wires. We noticed that numerous Bi liquid droplets formed (Fig. 1d-e) on top of PbSe nanoparticles grown on the TEM grid (Fig. 1g and Fig. S1), indicating that PbSe facilitates the condensation of Bi vapor and thus the formation of Bi droplets on the sidewall of the 1st PbSe wires to grow secondary branches (2nd PbSe wires).

To grow the 2nd PbSe wires, additional Bi precursors were added in the same sandwiched cell at room temperature. After heating at ~600°C, Bi deposited on the sidewalls of 1st PbSe wires (Fig. 1h-i), with the formation of a larger number of small Bi droplets and then the droplets coalesced with neighbors (Fig. 1i-j, denoted by cyan ellipses) to decrease surface energy, varying the branch density. After the Bi droplet formed on the 1st wires, 2nd PbSe wires started to grow (Fig. 1k, Fig. S2, and Movie S1). Similarly, the 3rd PbSe wires also grew via *in situ* TEM experiments (Fig. 1c and Fig. S3). During the branched wire growth, the wire width (d_W) became thinner and thinner from the 1st to 3rd wires (Fig. 1a-c), following $d_{W(n)} = (0.37 \sim 0.43) d_{W(n-1)}$ (n=2 to 3, denoting the 2nd and 3rd wires, Fig. 1l). Based on *ex situ* and *in situ* measurements, d_W was linearly scaled with d_S (d_W / d_s =0.57~0.63, Fig. 1l), in consistence with the theoretical estimation of ~0.51 from the balance among surface tensions at the VLS triple-phase junction (J_{TP}, Supplementary information (SI) -section 3). In addition, the wire width may not be constant during growth (S-section 4).

SEM images verified that branched wires grew on the sidewalls, {200} surfaces of PbSe wires (Fig. S6a-d) with the same crystal orientation (Fig. S6e-g). Both Se (~4.1 at.%, atomic percentage) and Pb (~5.5 at.%) were detected in catalyst droplets (Fig. S6h-j) in N_2 environment, while in our previous work, with the forming gas of 5% H_2 in N_2, Se forms H_2Se easily and thus no Se was detected in the catalyst droplet[21] (SI-section 5), presenting that the mass transport pathways of Se precursors can be tuned by environmental gas.

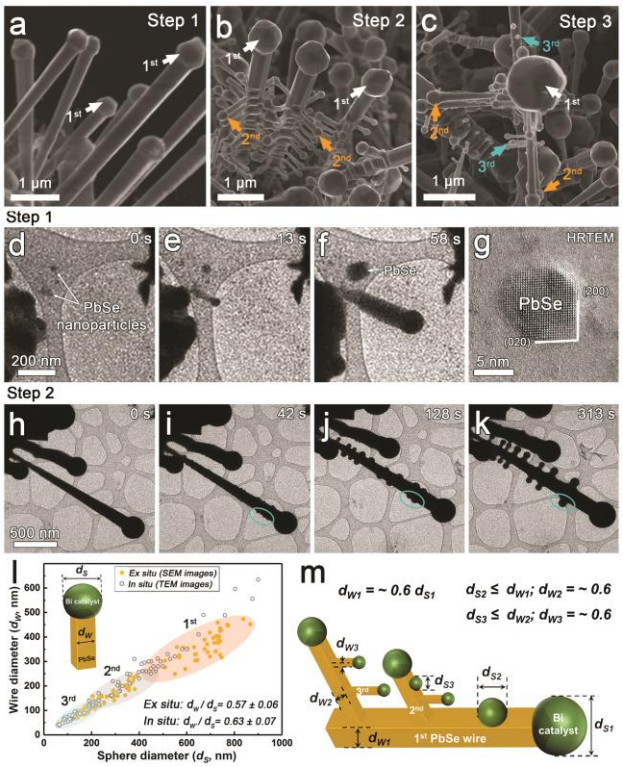

Fig. 1 Multi-step growth of PbSe branched wires. (a-c) SEM images of PbSe wires after the 1st, 2nd, and 3rd growth steps. (d-f) Time-sequenced BF-TEM images of PbSe wires during the 1st growth step. (g) The enlarged HRTEM image of one example of PbSe nanocrystals. (h-k) Time-sequenced BF-TEM images of the 2nd branched PbSe wires growth during the 2nd growth step. (l) Diameter distribution of catalyst spheres (d_S) and PbSe wires (d_W) measured based on SEM images and *in situ* TEM images showing a linear relationship between the catalyst droplet size and the width of the 1st, 2nd, and 3rd wires. (m) Schematic drawing of the relationship between the wire width and the catalyst droplet size of PbSe hierarchical structures.

The above described nucleation, growth, and coalescence processes of the catalyst droplets (Fig. 1j-k and Fig. S2) are closely related to the branch density of the structure. Therefore, we further investigated the process. Since the melting point of Bi (271°C[22]) is significantly lower than the reaction temperature (~ 600°C) providing a relative high equilibrium partial pressure of 1.9×10^{-1} Pa at 600 °C[23], we expect that Bi vapor pressure increased significantly after 271°C (Fig. S8). When supersaturation reached, Bi vapor condensed on the PbSe crystal surface with the formation of a large number of small catalyst droplets (Fig. 2a-b, and Fig. S2). The width of PbSe wires increased during the process at roughly three different rates (Fig. 2k) of 0.2-0.3 nm/s (0~80 s), 0.01-0.04 nm/s (80~150s), and 0.06-0.09 nm/s (>~150 s). We expect that the significant increase of wire width during initial ~80 s is due to the condensation of Bi vapor onto the sidewalls of 1st wires forming a thin film layer of Bi liquid. The thickness of the liquid layer can be estimated based on the initial d_{W1} (Fig. 2k, 0 s).When the thickness of the thin film reached 3~5 nm at ~ 33.8 s (Fig. 2b and k) the Bi droplets with a dome shape started to nucleate with a contact angle of <20° (Fig. 2i and j). The wire width barely grew after ~ 80 s, probably due to the significant growth of Bi droplets starting at ~55s (Fig. 2c) and the decrease of Bi deposition rate (Fig. 2c-e). The catalyst liquid thin film started to disappear after ~120 s when the contact angle is ~85° (Fig. 2i and k), which is close to the estimated equilibrium contact angle (96.6°) between the catalyst droplet and the wire sidewall (SI-section 6). In addition, the contact angles varied from ~ 10° to ~ 85° (Fig. 2i) further confirming the formation of a thin layer of Bi liquid at the beginning and its transition from thin film to liquid droplets. The unequal contact angles at two sides of each catalyst droplet (Fig. 2i) lead to the motion of droplets[24, 25] and thus coalescence (Fig. 2g-h and Fig. 2c-e) to decreases surface

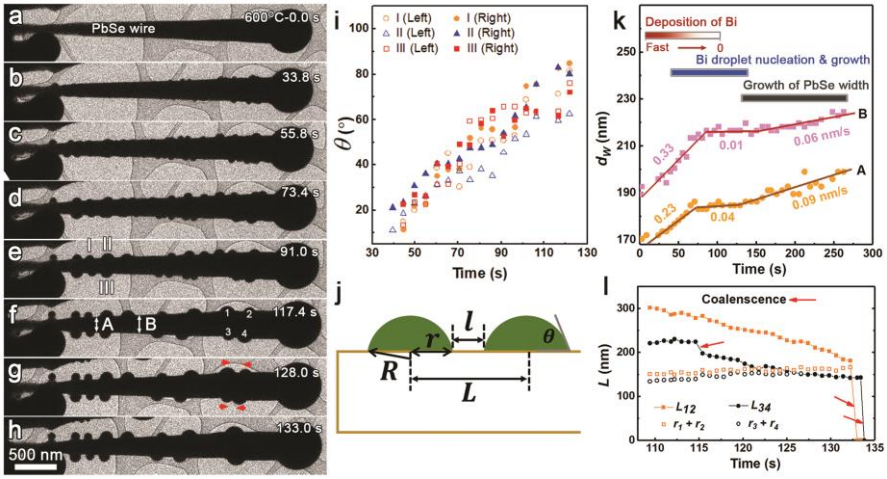

Fig. 2 Nucleation and coalescence processes of liquid catalysts on the sidewall of the 1st PbSe wire. (a-h) Time-sequenced of *in situ* TEM BF images showing the nucleation, growth, and coalescence processes of Bi liquid catalyst on the sidewall of PbSe wires. (i) Measured contact angle (left and right sides) of liquid catalyst droplets I, II, and III in (e) at various times during the heating process. (j) Schematic illustration of measurement parameters. r is the radius of the circle interface between Bi liquid and PbSe solid. (k) Wire width evolution at locations A and B in (f). (l) Evolution of L and r of between Bi droplets 1 and 2, and droplets 3 and 4 in (f). R is the radius of the catalyst droplet sphere. r is the radius of the interface between droplet and PbSe solid. L is distance between two closed catalyst droplets. Notably, TEM images present 2D projection. Although it seems that droplets 3 and 4 are overlapped at ~126 s (Fig. 2l), they are at different height and do not merge until 133.8 s.

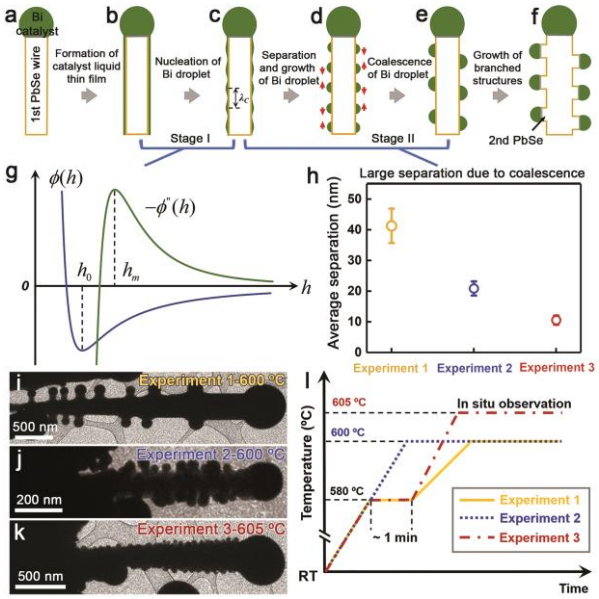

Figure 3. Processes of nucleation, growth, and coalescence of catalyst droplets and corresponding theories. (a-f**)** Schematic illustration of the proposed formation process of Bi liquid catalyst droplets on the sidewall of a PbSe wire showing two stages of catalyst evolution before VLS growth of PbSe branched structures. (g**)** Calculation of $\phi(h)$ between L/S and V/S interfaces and second derivative $-\phi''(h)$ that permits spinodal de-wetting (stage I). (h) Experimental measurements of l vs. R showing large l due to coalescence. (i-k) TEM images of wires grown under various heating conditions. (l) Schematic drawing of temperature setups for experiments 1, 2, and 3. Note, temperature ramping rate cannot be controlled digitally and thus controlled manually by holding temperature at 580ºC for 1 min to slow ramping rate.

energy[26]. After ~120 s, the branches started to grow and the width of 1st wires increased slowly at a rate of and 0.06-0.09 nm/s (Fig. 2k) by deposition of Pb and Se on the sidewalls after the liquid thin film disappeared.

Based on the above analysis, the droplet growth process resembles the kinetically limited Stranski-Krastanov (SK) growth mode[27, 28], in which the initial layer-by-layer film growth transitions to the island growth behavior at the later stage. For the system studied here, the observed film-to-island transition results from the de-wetting of the Bi liquid film[29], and specifically through the spinodal de-wetting process[30-32] when the film reaches a critical thickness (3~5 nm at ~33 s) and becomes unstable against periodic perturbation to film thickness as illustrated in Fig. 3a-c. Spinodal de-wetting is driven by the long-range force such as van der Waals force across the liquid film. The critical wavelength of the resultant film perturbations, which gives the lower limit of the nuclei separation seen in Fig. 3c, can be written as: $\lambda_C = 2\pi\sqrt{-\gamma / \phi''(h)}$ (see derivation in SI-section 7). Here, γ is the liquid surface energy, h is liquid film thickness, and $\phi(h)$ is the effective interaction potential between the two surfaces of the liquid film. $-\phi''(h)$ is the second derivative of $-\phi(h)$. As shown in Fig. 3g, spinodal de-wetting is most favored to develop kinetically at $h = h_m$, at which its driving force $-\phi''(h)$ is maximized. With an estimate of h_m = ~4 nm based on experiment, λ_C is found to be 16 – 23 nm (see SI-section 7), which is in reasonable agreement with the observed distances between Bi liquid droplets. While spinodal de-wetting has been utilized to generate nanoscale patterns on flat substrates[33], here we show that this phenomenon can be exploited to catalyst droplet nucleation in VLS growth of hierarchical nanostructures. Because λ_C is h-dependent and scales with h quadratically at large film thickness (SI-section 7), the droplet spacing can be tuned by the Bi deposition rate or vapor supply.

In addition, the coalescence of catalyst droplets can be kinetically controlled by governing partial pressure of growth species, temperature, and temperature increasing rate. In contrast to experiment 1 (Fig. 3i and l), high branch density was obtained by increasing temperature ramping rate (experiment 2, Fig. 3j and l) or temperature (experiment 3, Fig. 3k and l), which provide supersaturation of PbSe growth species before coalescence of catalyst droplets leading to high branch density.

Besides the branch density, we also found that the catalyst droplet affected the wire growth (Fig. 4). For a single wire, the size of the droplets varies with time but the wire shows a similar growth rate overall with slight variation (Fig. 4b). This seems to be consistent with a previous study[15]. However, we cannot unambiguously conclude that the wire growth rate is independent with catalyst size. Different catalyst sizes show different wire growth rates for three different wires grown simultaneously at the same location (Fig. 4c). Conversely, at a given catalyst size (94.5 nm) but different times, the three different wires show different growth rates (Fig. 4d). This clearly indicates a temporal variation of the growth environment. Therefore, we expect that the partial pressures of precursors are not constant with time in this system. Overall, the smaller the catalyst droplet size, the faster the growth rate (Fig. 4c), inconsistent with previous reports of

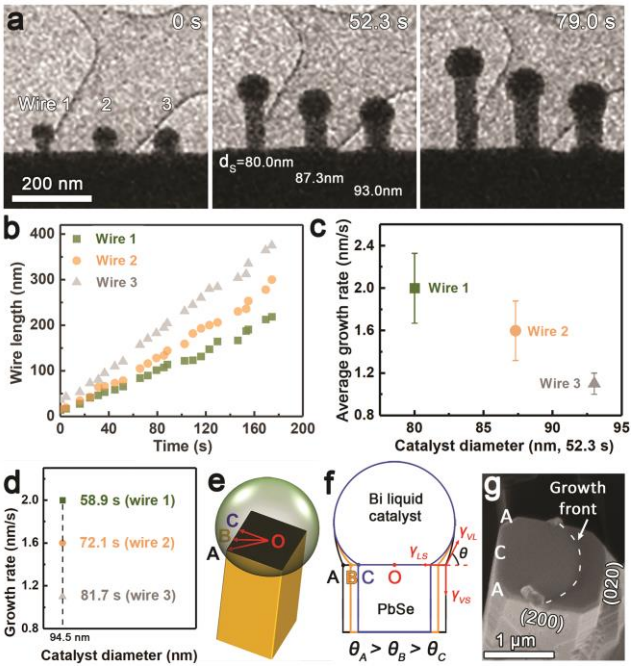

Fig. 4 The effects of the radius of curvature on the wire growth. (a) *In situ* observation of the simultaneous growth of three 2nd PbSe wires with different catalyst droplet sizes at the same location. (b) Wire length of three wires in (a) vs. time showing the smaller catalyst droplet, the larger the wire growth rate. (c) Relationship between the catalyst diameters (ds, at 52.3 s) and wire growth rates. Error bars indicate standard error. (d) Variation of growth rates of three wires in (a), which had the same catalyst size but grew at different times. (e) Schematic illustration of the growth interface (L/S) with three different locations of A, B, and C. (f) Cross-section views at different JTP, along OA, OB, and OC in (f) showing curvature variation with different angles of $\theta_A > \theta_B > \theta_C$. (g) An SEM image showing the growth interface (L/S) with a curved growth front.

Gibbs-Thomson effect[12, 16] on growth rate of single element wires. In the case of our compound wire growth and complicated growth environment, we propose that the difference in growth rate are possibly affected by (1) mass transport pathways and (2) atomic surface diffusion. As we previously reported, Pb is miscible in Bi bulk liquid above 327 °C (Fig. S8) and we observe a sufficient amount (up to 85 at%) of Pb, but not Se, in liquid Bi catalyst droplet via in situ TEM experiments[21]. Therefore, the mass transport of Pb precursor is possibly affected by the chemical potential of Pb in Bi liquid and PbSe solid, unlike the Gibbs-Thomson-effect controlled growth (e.g. Ge wire growth with Au as the catalyst), where the supersaturation, the driving force of wire growth, is the difference between the chemical potential of growth species in the vapor and solid phases[16]. In the liquid catalyst droplets, the small radius of curvature (high chemical potential) possibly reduces the solubility of the growth precursors[14]. Correspondingly, the supersaturation of growth species inside small droplets is higher than that inside large droplets under the same vapor environment, leading to a fast growth rate under the assumption that mass transport of Pb kinetically controls the growth of PbSe wire (Fig. 4c).

We observe the variation of wire diameters during growth (Fig. S5), indicating possible atomic deposition and diffusion on the side wall surfaces. We propose that another possible factor that affects PbSe nanowire growth rate is atomic diffusion on the surface, consistent with the InP or GaAs growth process[34], during which, when wire diameters are above ~50 nm, the larger the wire size the lower the wire growth rate.

In addition, the curvature within one droplet also varies, because PbSe wires are faceted with {200} planes as sidewalls during growth at 600°C instead of the generally hypothesized circle[35, 36]. This was verified by (i) the wire width remains almost the same at room and high temperatures considering the thermal expansion of PbSe crystal (Fig. S7), indicating that the morphology of the wires does not change from circular cylinder to square cuboid; (ii) at room temperature, PbSe wires are faceted with {200} sidewalls (Fig. 4g and Fig. S6). Therefore, the S/L interface has a square shape, leading to the variation of the contact angle at J_{TP} along the periphery of the interface (Fig. 4e). For example, the curvature of liquid catalyst droplet is getting larger and larger from locations A to B to C (Fig. 4e and f). As previously reported[21], PbSe nucleated at the edge of the interface between Bi liquid droplet and PbSe solid and grew across the {002} plane of PbSe via the layer-by-layer mechanism. At location C, PbSe nucleates faster with smaller radius of curvature than at location A, forming a curved growth front step on the growth interface (Fig. 4g). The diffusion difference between the bulk and near the surface of the liquid droplet[37] may also lead to the different growth rates along A to C locations, but the nucleation step kinetically dominates the layer-by-layer growth because the nucleation time is significantly longer than that of the lateral layer growth time[38]. This curved growth front is consistent with the analysis of the effect of catalyst droplet size on wire growth rate.

In summary, our work reveals the kinetic information of the nucleation, growth, and coalescence process of Bi liquid catalyst droplets and the dependence of catalyst droplets on the branch growth and the resulting branch structures. By understanding this formation mechanism of catalyst droplets, we tailored the branch density by kinetically tuning the growth process, such as varying the feed of growth species via temperature control. The analyses reported herein, highlight that the catalysts during VLS growth of branched structures not only increase the rate of the reaction but also has a strong correlation with the growth process and the resulting hierarchical structures. The findings suggest that the mass transport pathways of growth species can be tuned by changing environmental gas, providing a potential strategy to manipulate both the structure and composition of hierarchical structures, which has been extensively employed in energy conversion and storage devises[9, 39], gas sensor[40], and catalytic reaction[41] due to their tunable 3D morphology and homo or heterogeneous junction, high surface-to-volume ratios, and effective light absorption, etc. Our findings can be extended to other VLS systems enabling the possibility of controlling the growth of various hierarchical structures, such as Ga(N, P, Sb)[10, 42, 43], GeSn[44], ZnO[40], CdS[45], SnO_2[46], with tailored structures and compositions and thus the desired properties.

Conflicts of interest

There are no conflicts to declare.

Acknowledgement

This research was supported by the U.S. Department of Energy (DOE), Office of Science, Office of Basic Energy Sciences (BES), Early Career Research program under Award KC0203020:67037. The theoretical calculation was supported by DOE BES under project number DE-SC0019111. Theoretical analysis of nucleation and coalescence was partially supported by the DOE BES Materials Sciences and Engineering Division (DMSE). Y.Z. and M.T. acknowledge support by DOE BES under project number DE-SC0019111. The work was conducted in the William R. Wiley Environmen-tal Molecular Sciences Laboratory (EMSL), a national scientific user facility sponsored by the DOE Office of Biological and Environmental Research and located at Pacific Northwest Na-tional Laboratory (PNNL). PNNL is a multiprogram national laboratory operated for the U.S. Department of Energy by Bat-telle under Contract No. DE-AC05-76RLO1830.

References

1. H. B. Wu, J. S. Chen, X. W. Lou and H. H. Hng, *J. Phys. Chem. C*, 2011, **115**, 24605-24610.
2. H. E. Jeong, S. H. Lee, J. K. Kim and K. Y. Suh, *Langmuir*, 2006, **22**, 1640-1645.
3. Y. C. Jung and B. Bhushan, *ACS Nano*, 2009, **3**, 4155-4163.
4. S. Yin, Y. Zhang, J. Kong, C. Zou, C. M. Li, X. Lu, J. Ma, F. Y. C. Boey and X. Chen, *ACS Nano*, 2011, **5**, 3831-3838.
5. J. Zhu, H. Peng, C. K. Chan, K. Jarausch, X. F. Zhang and Y. Cui, *Nano Lett.*, 2007, **7**, 1095-1099.
6. W. Zhou, C. Cheng, J. Liu, Y. Y. Tay, J. Jiang, X. Jia, J. Zhang, H. Gong, H. H. Hng, T. Yu and H. J. Fan, *Adv. Funct. Mater.*, 2011, **21**, 2439-2445.
7. K. Miszta, J. de Graaf, G. Bertoni, D. Dorfs, R. Brescia, S. Marras, L. Ceseracciu, R. Cingolani, R. van Roij, M. Dijkstra and L. Manna, *Nat. Mater.*, 2011, **10**, 872-876.
8. M. J. Bierman, Y. K. A. Lau, A. V. Kvit, A. L. Schmitt and S. Jin, *Science*, 2008, **320**, 1060-1063.
9. C. Cheng and H. J. Fan, *Nano Today*, 2012, **7**, 327-343.
10. C. Yan, X. Li, K. Zhou, A. Pan, P. Werner, S. L. Mensah, A. T. Vogel and V. Schmidt, *Nano Lett.*, 2012, **12**, 1799-1805.
11. J. Zhu, H. Peng, A. F. Marshall, D. M. Barnett, W. D. Nix and Y. Cui, *Nat. Nanotechnol*,2008, **3**, 477-481.
12. E. I. Givargizov, *J. Cryst. Growth*, 1973, **20**, 217-226.
13. J. Kikkawa, Y. Ohno and S. Takeda, *Appl. Phys. Lett.*, 2005, **86**, 123109.
14. V. A. Nebol'sin, A. A. Shchetinin, A. A. Dolgachev and V. V. Korneeva, *Inorg. Mater.*, 2005, **41**, 1256-1259.
15. S. Kodambaka, J. Tersoff, M. C. Reuter and F. M. Ross, *Phys. Rev. Lett.*, 2006, **96**, 096105.
16. S. A. Dayeh and S. T. Picraux, *Nano Lett.*, 2010, **10**, 4032-4039.
17. V. G. Dubrovskiĭ, N. V. Sibirev, R. A. Suris, G. É. Cirlin, V. M. Ustinov, M. Tchernysheva and J. C. Harmand, *Semiconductors*, 2006, **40**, 1075-1082.

18. S. A. Dayeh, E. T. Yu and D. Wang, *Nano Lett.*, 2009, **9**, 1967-1972.
19. V. G. Dubrovskii, Y. Berdnikov, J. Schmidtbauer, M. Borg, K. Storm, K. Deppert and J. Johansson, *Cryst. Growth Des.*, 2016, **16**, 2167-2172.
20. M. T. Borgström, G. Immink, B. Ketelaars, R. Algra and E. P. A. M. Bakkers, *Nat. Nanotechnol*, 2007, **2**, 541-544.
21. M. Song, J. Lee, B. Wang, B. A. Legg, S. Hu, J. Chun and D. Li, *Nanoscale*, 2019, **11**, 5874-5878.
22. T. B. Massalski, H. Okamoto and P. R. Subramanian, *Binary alloy phase diagrams*, ASM International, 2, illustrated, reprint edn., 1990.
23. A. K. Fischer, *The Journal of Chemical Physics*, 1966, **45**, 375-377.
24. M. K. Chaudhury and G. M. Whitesides, *Science*, 1992, **256**, 1539.
25. F. Brochard, *Langmuir*, 1989, **5**, 432-438.
26. F. Blanchette and T. P. Bigioni, *Nat. Phys*, 2006, **2**, 254-257.
27. A. Baskaran and P. Smereka, *J. Appl. Phys.*, 2012, **111**, 044321.
28. A. Winkler, *Surf. Sci.*, 2016, **652**, 367-377.
29. A. M. J. Edwards, R. Ledesma-Aguilar, M. I. Newton, C. V. Brown and G. McHale, *Sci. Adv*, 2016, **2**, e1600183.
30. J. Bischof, D. Scherer, S. Herminghaus and P. Leiderer, *Phys. Rev. Lett.*, 1996, **77**, 1536-1539.
31. S. Herminghaus, K. Jacobs, K. Mecke, J. Bischof, A. Fery, M. Ibn-Elhaj and S. Schlagowski, *Science*, 1998, **282**, 916-919.
32. R. Xie, A. Karim, J. F. Douglas, C. C. Han and R. A. Weiss, *Phys. Rev. Lett.*, 1998, **81**, 1251-1254.
33. D. Gentili, G. Foschi, F. Valle, M. Cavallini and F. Biscarini, *Chem Soc Rev*, 2012, **41**, 4430-4443.
34. V. G. Dubrovskii, N. V. Sibirev, G. E. Cirlin, I. P. Soshnikov, W. H. Chen, R. Larde, E. Cadel, P. Pareige, T. Xu, B. Grandidier, J. P. Nys, D. Stievenard, M. Moewe, L. C. Chuang and C. Chang-Hasnain, *Phys. Rev. B*, 2009, **79**, 205316.
35. E. J. Schwalbach and P. W. Voorhees, *Nano Lett.*, 2008, **8**, 3739-3745.
36. C. Y. Wen, J. Tersoff, M. C. Reuter, E. A. Stach and F. M. Ross, *Phys. Rev. Lett.*, 2010, **105**, 195502.
37. H. Wang, L. A. Zepeda-Ruiz, G. H. Gilmer and M. Upmanyu, *Nat Commun*, 2013, **4**, 1956.
38. C. Y. Wen, M. C. Reuter, J. Bruley, J. Tersoff, S. Kodambaka, E. A. Stach and F. M. Ross, *Science*, 2009, **326**, 1247-1250.
39. M. J. Bierman and S. Jin, *Energy Environ. Sci.*, 2009, **2**, 1050-1059.
40. H.-S. Woo, C.-H. Kwak, J.-H. Chung and J.-H. Lee, *Sens. Actuators B Chem.*, 2015, **216**, 358-366.
41. I. S. Cho, Z. Chen, A. J. Forman, D. R. Kim, P. M. Rao, T. F. Jaramillo and X. Zheng, *Nano Lett.*, 2011, **11**, 4978-4984.
42. D. Wang, F. Qian, C. Yang, Z. Zhong and C. M. Lieber, *Nano Lett.*, 2004, **4**, 871-874.
43. K. A. Dick, K. Deppert, M. W. Larsson, T. Mårtensson, W. Seifert, L. R. Wallenberg and L. Samuelson, *Nat. Mater.*, 2004, **3**, 380-384.
44. J. Doherty, S. Biswas, D. McNulty, C. Downing, S. Raha, C. O'Regan, A. Singha, C. O'Dwyer and J. D. Holmes, *Chem. Mater.*, 2019, **31**, 4016-4024.
45. Y. Jung, D.-K. Ko and R. Agarwal, *Nano Lett.*, 2007, **7**, 264-268.
46. S.-W. Choi, A. Katoch, G.-J. Sun and S. S. Kim, *Sens. Actuators B Chem.*,2013, **181**, 787-794.